Robust Self-healable and 3D-Printable Waterborne Polyurethane

Highlights

This chapter reveals another easy but impactful tactic to achieve a robust SHWPU elastomer with excellent healing efficiency along with other vital properties obligatory to consider it as an advanced material. Notably, the tactic is to deploy the mutual effects of 'dynamic hard domains (2-aminophinyl disulfide, 2-APDS)', 'asymmetric (isophorone diisocyanate-isophorone diamine, IPDI-IPDA) architecture', and 'shape memory effect (SME)' in a single material. The loosely packed IPDI-IPDA moieties and SME promotes the reversible S-S metathesis reactions, resulting in high healing efficiency as well as high mechanical strength, simultaneously. Based on this tactic, a series of robust self-healable WPUs (SHWPUs) was synthesized with good healing efficiency (70.22-79.94%), shape recovery (88.4-97.4%), excellent mechanical strength (16.09-26.23 MPa), high elongation at break (1604-2071%), outstanding toughness (188.3-216.6 MJm^{-3}), high fracture energy (46.74-66.33 kJm^{-2}), good biocompatibility, and acceptable biodegradability. Outstandingly, an SHWPU film could lift a dumbbell of 25 kg, which is 53648 times heavier than its weight without any crack. Taking advantage of good shape-recoverability, the elastomer was tested for 'artificial muscle' contraction. Impressively, a presentative SHWPU film could vertically and successfully lift a 100 g load which is 251.19 times heavier than its weight under ambient conditions. Moreover, a series of 3D printable gelatin/SHWPU ink was prepared which possesses the potential for bone scaffolds. Additionally, this thermoplastic SHWPU could be reprocessed at 80 °C under 60-80 kg cm^{-2} pressure.

Parts of this chapter are published in

Morang, S., Bandyopadhyay, A., Rajput, J.H., Mandal, B.B., Poundarik, A. and Karak, N. Robust self-healable and three-dimensional printable thermoplastic elastomeric waterborne polyurethane for artificial muscle and biomedical scaffold applications. *ACS Applied Polymer Materials*, 5(10):8518–8532, 2023. (DOI: 10.1021/acsapm.3c01627)


ACS APPLIED POLYMER MATERIALS

pubs.acs.org/acsapm Article

Robust Self-Healable and Three-Dimensional Printable Thermoplastic Elastomeric Waterborne Polyurethane for Artificial Muscle and Biomedical Scaffold Applications

Samiran Morang, Ashutosh Bandyopadhyay, Jay Hind Rajput, Biman B. Mandal, Atharva Poundarik, and Niranjan Karak*

Cite This: https://doi.org/10.1021/acsapm.3c01627 Read Online

5.1. Introduction

From **chapter 4**, it is evident that waterborne polyurethane (WPU) with asymmetric architecture exhibited excellent mechanical properties including extreme stretchability, good self-healing (SH), shape memory (SM), and reprocessability attributes. However, superior applications demand more advancement in their inherent properties. Hence, WPU needed to be improved via precise molecular engineering.

As mentioned in the earlier chapters, self-healable WPU (SHWPU) can spontaneously heal physical damages and restore mechanical performances, which prolongs its lifespan and reduces energy consumption, maintenance cost, and waste generation [1]. However, the prerequisites for high mechanical performance, such as high molecular chain rigidity, intermolecular interactions, and crystallinity are innately contradictory to the necessary molecular arrangement or bond re-association-dissociation for chain mobility and exchange of reversible bonds for good self-healing. To answer this dilemma, we introduced an easy but impactful strategy into WPU matrix, which is based on the triple synergistic effect of 'dynamic hard domains (2-aminophenyl disulfide, 2-APDS)', 'asymmetric IPDI-IPDA (isophorone diisocyanate-isophorone diamine) architecture', and 'shape memory effect (SME)'. In this study, a series of robust SHWPUs from monoglyceride of castor oil (MG_{CO}), glycerol ester of citric acid (GECA), 2-aminophenyl disulfide (2-APDS) along with other desired reactants. The loosely packed IPDI-IPDA moieties and SME promotes the reversible S-S metathesis reactions, resulting in high healing efficiency as well as mechanical strength, simultaneously. The semi-crystalline ε-polycaprolactone diol (ε-PCL_{2000}) induces the shape recovery ability by developing a microphase-separated structure (hard-soft) with hard domains. Again, the fabricated GECA not only plays the role of internal emulsifier but also encourages shape memory behavior via chemical cross-linking with the help of its four wings of hydroxyl groups. Most essentially, the biocompatibility nature of the SHWPUs was established by platelet adhesion study, lactate dehydrogenase (LDH) activity, erythrocyte or red blood corpuscle (RBC) lysis, cellular viability (live/dead) assay, and cell proliferation (Alamar blue) assay using human dermal fibroblasts (HDFs) seeded on the elastomeric PUs.

Presently, 3D bio-printing is a prominent technology that can fulfill the mechanical and biological requirements of material properties for developing a medical device. Gelatin and its derivatives have been majorly used in tissue engineering where thermo-responsiveness, cell adhesion, shear thinning, and biocompatibility are needed. Gelatin based scaffold properties can improve by incorporating appropriate compatible synthetic or natural polymers [2]. In the 3D bio-printing making the printable composition of natural polymers with synthetic polymer is still challenging due to their low compatibility in terms

of forming a homogeneous mixture, nozzle clogging during printing, phase separation, chemically reactive to form by-products, difficulty controlling the viscosity of the mixed solution, environmental conditions, and operating parameters. In comparison PCL, poly(lactic acid) (PLA), and natural polymers, WPU remains less investigated in 3D bio-printing despite having good mechanical properties and biocompatibility [3]. So, we have explored the usability of SHWPU dispersion as the main component of 3D printable Gelatin/SHWPU ink for biological applications like bone scaffolds. Gelatin was used to improve printability at various concentrations. Furthermore, the developed elastomer showed potential in artificial muscles and was verified by the weight-lifting test. Therefore, in this report a bio-based tough self-healable and 3D-printable thermoplastic elastomeric WPU is reported for artificial muscle and biomedical scaffold applications.

5.2. Experimental

5.2.1. Materials

In this study starting materials including, IPDI, ε-PCL_{2000}, 2,2-bis(hydroxymethyl) propionic acid (DMPA), 2-APDS, citric acid, glycerol, castor oil, triethyl amine (TEA), *para*-toluene sulphonic acid (*p*-TSA), calcium oxide (CaO), N, N-dimethylformamide (DMF), and dibutyltin dilaurate (DBTDL) are used for preparing SHWPU dispersions. All these chemicals have the same specifications as discussed in the **Chapter 3** and **Chapter 4**.

5.2.2. Methods

5.2.2.1. Preparation of monoglyceride of castor oil (MG_{CO})

MG_{CO} was prepared from the reaction between castor oil and glycerol, using CaO as the catalyst as discussed in **Chapter 2**, **section 2.2.2.1**.

5.2.2.2. Preparation of glycerol ester of citric acid (GECA)

GECA was prepared the reaction between citric acid and glycerol, using *p*-TSA as the catalyst as mentioned in **Chapter 2**, **section 2.2.2.2**.

5.2.2.3. Preparation of self-healable waterborne polyurethane (SHWPU)

Four different types of SHWPUs were prepared via pre-polymerization techniques as stated in **Chapter 4**, using the same chemicals and varying S-S content i.e., 2-APDS amount. Stepwise, the only difference is that the 2-APDS was added just 1 h before the neutralization step. The optimized chemical composition for SHWPUs is tabulated in **Table 5.1**. The resultant dispersions were cast on different surfaces (e.g., Teflon sheet, steel plates) as per the requirements of the testing and analyses.

Table 5.1. Chemical compositions of the reactants for preparing SHWPU dispersions.

Reactants	SHWPU-1 (mM)	SHWPU-2 (mM)	SHWPU-3 (mM)	SHWPU-4 (mM)
ε-PCL	1.5	1.5	1.5	1.5
DMPA	1.5	1.5	1.5	1.5
MG_{CO}	1	1	1	1
GECA	0.375	0.375	0.375	0.375
2-APDS	0.575	1.15	1.725	2.875
IPDA	0.35	0.35	0.35	0.35
IPDI	6.175	6.750	7.325	8.475
TEA	1.972	1.972	1.972	1.972

5.2.3 Characterization and tests

5.2.3.1. Structural characterization and property evaluation

Different characterization methods and tests that were followed and employed to investigate and evaluate important properties of the developed SHWPUs are same as mentioned in the C**hapter 2**, **Chapter 3,** and **Chapter 4**.

The shape recovery and shape fixity under heat and microwave irradiation were calculated using the following equations.

$$\text{Shape fixity } (\%) = \frac{\theta}{90} \times 100 \qquad \textbf{Eq. 5. 1}$$

$$\text{Shape recovery } (\%) = \frac{90 - \theta}{90} \times 100 \qquad \textbf{Eq. 5. 2}$$

Here, θ corresponds to the angle between the tangential line at the middle point of the specimen and the line connecting the middle point and the edge of the ring or spiral shape.

5.2.3.2. *In vitro* hemocompatibility study

The hemocompatibility study was carried out following same procedure and protocol as described in **Chapter 4**, **Section 4.2.3.4**.

5.2.3.3. *In vitro* degradation study

The *in vitro* degradation study investigated following same method as mentioned in **Chapter 4**, **Section 4.2.3.5**.

5.2.3.4. *In vitro* cytocompatibility and cell proliferation study

The *in vitro* cytocompatibility and cell proliferation study was scrutinized following same protocol and methods as illustrated in **Chapter 4**, **Section 4.2.3.6**.

5.2.3.5. SHWPU elastomer as artificial muscle

To investigate its potential as an artificial muscle, a rectangular shape SHWPU-1 film (0. 39811g, length 40 mm × width 8 mm × thickness 0.8 mm) was used in this test. In the first step, the film was stretched 250% (2.5 times its original length) after heating the sample at 80-85 ℃for 10 min. Afterward, the elongated length was fixed by placing the same film inside a Refrigerator (-3 ℃). Both ends of the film were capped with two dovetail clips. One end of this capped film was tethered while the other was loaded with a weight of 100 g before applying heat treatment from 80 to 90 ℃. In the final step, the sample was placed in a convection oven at the specified temperature and allowed to restore the original shape.

5.2.3.6. Fabrication of gelatin/SHWPU-2 scaffold using 3D bio-printer

An ANGA PRO 3D bioprinter (ALFATEK SYSTEMS, Twin extruder) was used for the printing of gelatin/SHWPU-2 scaffolds. Gelatin 0.2% (wt/v) solution was first made at 40–50 °C by stirring it for 30–50 min. Subsequently, a homogenous mixture of the gelatin 0.2% (wt/v) solution and SHWPU-2 dispersion was prepared at volume ratios of 1:0.3 and 1:0.5. Thereafter, a 22 G conical tapered tip of the Luer syringe was affixed in the bioprinter before the gelatin/SHWPU-2 mixture was taken in it. The gelatin/SHWPU-2 mixture was kept at ambient temperature for a few minutes until the solution became extrudable (partially solidified, viscous); before the commencement of the bioprinting. The cuboid design (3.5 cm × 3.5 cm × 2 cm) was created with the help of SOLIDWORKS 2021 design software in. amf (additive manufacturing file), while Cura_14.09 software was used for slicing the cuboid design. Further, converted. amf to G. Code file with optimized parameters was used for the printing, and the scaffolds were made on the collector.

5.2.3.7. Biodegradation test

The biodegradability of SHWPUs films was scrutinized by soil burial method as stated in **Chapter 3, Section 4.2.3.7**.

5.3. Results and discussion

5.3.1. Preparation and characterization of SHWPUs

As shown in **Scheme 5.1**, a series of SHWPU elastomers was synthesized using a pre-polymerization method from the calculated amount of ε-PCL_{2000}, DMPA, GECA, MG_{CO}, 2-APDS, IPDI, and IPDA under appropriate conditions. Different chemical reactions took place among the components and the various interactions that resulted in the product are shown in **Scheme 5.1. (b)**.

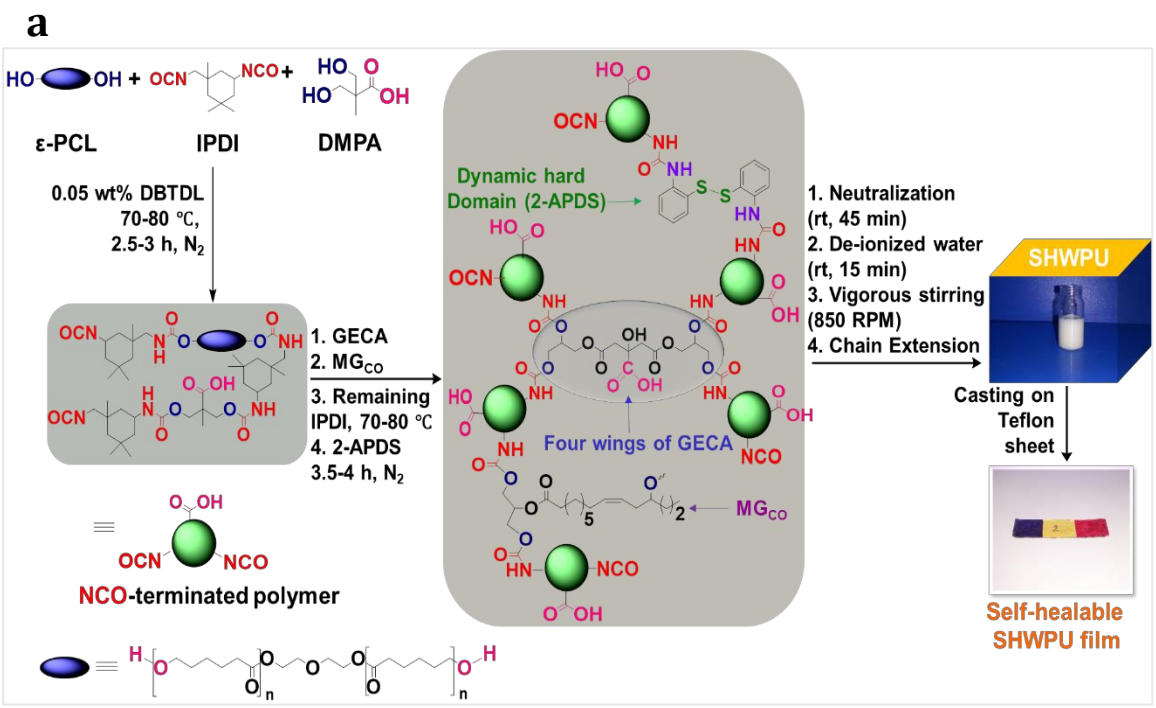

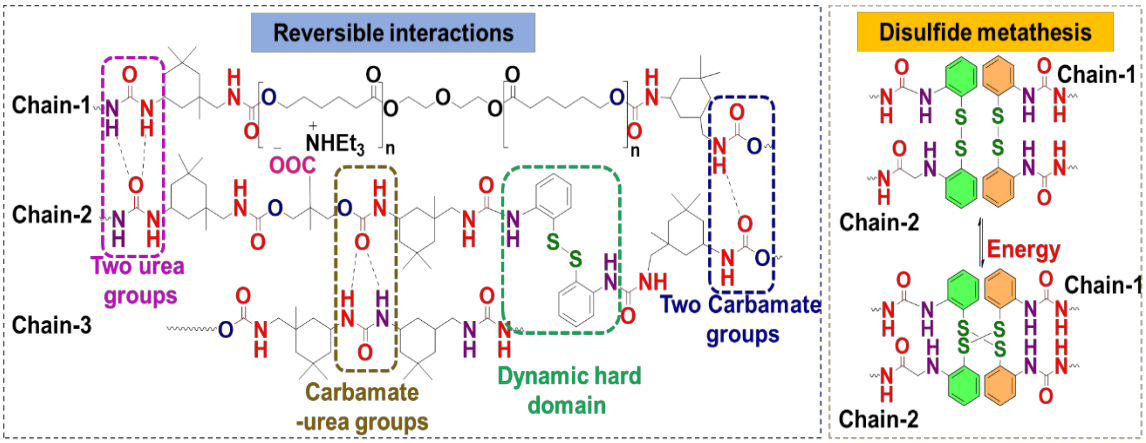

Scheme 5.1. (a) Steps involved for preparing SHWPU (rt = room temperature) and (b) possible reversible interactions (covalent and non-covalent) and disulfide metathesis in SHWPU.

Each of these components has its unique function. Precisely, the semi-crystalline ε-PCL_{2000} acts as the soft segment, DMPA, and GECA as an internal emulsifier, 2-APDS as the dynamic but hard moiety, and IPDA and MG_{CO} as the chain extenders. The disulfide metathesis and possible dynamic reversible interactions have been developed between various groups of the polymeric chains. The intensity of these interactions is closely associated with the inherent properties of SHWPU as discussed in the subsequent sections. The obtained dispersions, as well as the desired elastomers, were characterized by the standard techniques discussed here. An FTIR peak near 2276 cm^{-1} corresponds to the free isocyanate groups of WPU prepolymer (SHWPU) as shown in **Figure 5.1**. Noticeably, the same peak did not appear in the respective FTIR spectra of SHWPUs. So, it is clear that all isocyanates reacted with hydroxyl groups and amine groups to form carbamate or urethane linkages and urea linkages, respectively.

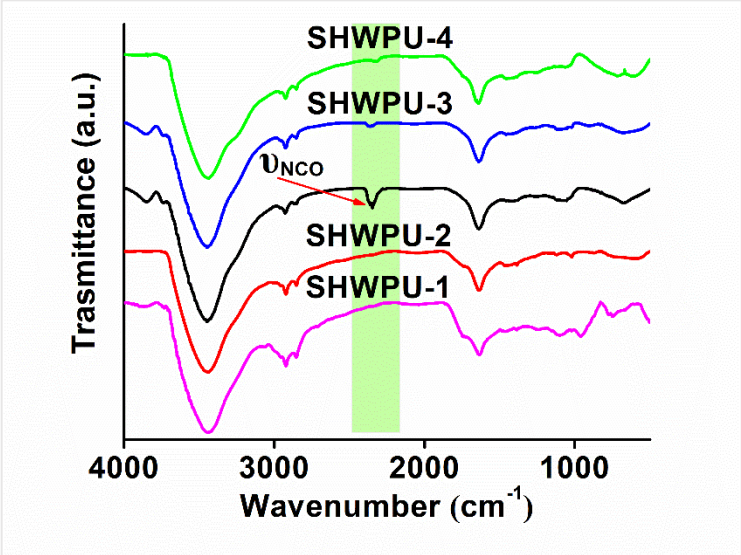

Figure 5.1. FTIR spectra of SHWPU-1 prepolymer and SHWPUs.

For free –OH, the stretching band should be observed in the range of 3550-3500 cm^{-1} which was not observed, instead of that a broad peak near 3445 cm^{-1} appeared which corresponds to –NH or hydrogen-bonded -OH stretching vibration. Two peaks at 2819 cm^{-1} and 2859 cm^{-1} can be accredited to the symmetric and asymmetric vibrational stretching frequencies of –CH groups, respectively. The stretching frequencies of -C=O groups of carbamate moiety were found at 1736 cm^{-1} and 1637 cm^{-1}. Again, multiple peaks near 1239-952 cm^{-1} can be assigned to the C-O stretching frequency. Furthermore, a small peak near 1393 corresponds to –CH bending vibration. A combination of these FTIR data supports the formation of a PU matrix, diminutively [4]. A perusal of **Figure 5.2 (a)** and **(b)** demonstrated the obtained ^{1}H and ^{13}C NMR spectra for SHWPU-2. In **Figure 5.2 (a)**, the chemical shift value at δ= 0.87-1.31 ppm (a & b, $-CH_3$) can be assigned to the free methyl groups of IPDI and IPDA.

Again, α and β methylene protons concerning ester groups (towards the C atom) of ε-PCL moiety, appeared at δ= 2.26-2.29 ppm (d, -CH_2) and δ= 1.51-1.57 ppm (c, -CH_2), respectively.

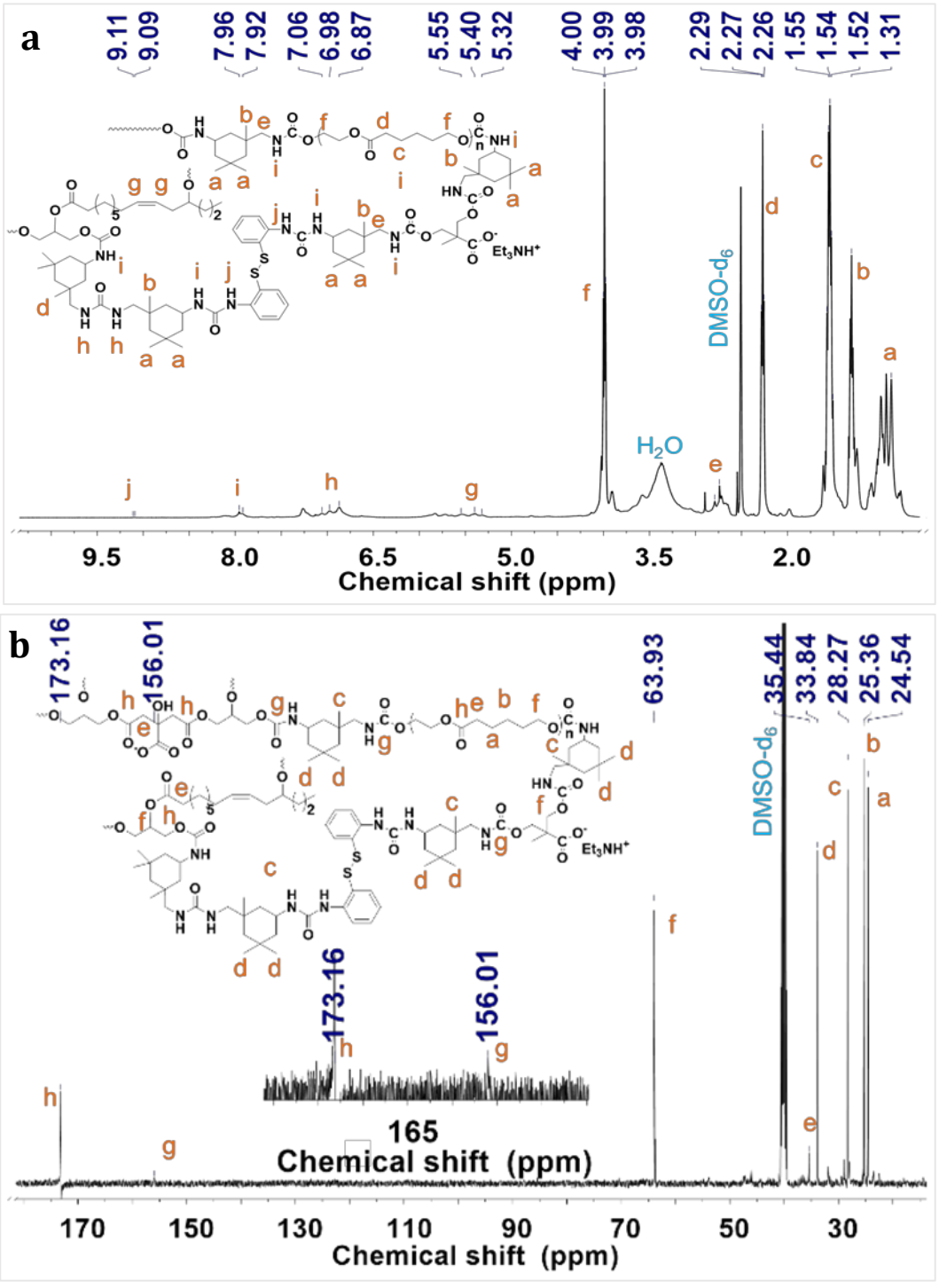

Figure 5.2. (a) ^{1}H and (b) ^{13}NMR spectra of SHWPU-2.

A doublet at δ= 2.74-2.79 ppm (e, -CH_2) and a sharp triplet at δ= 3.98-4.00 ppm (f, CH_2) can be accredited to the methylene proton attached and adjacent to urethane moiety, respectively. The chemical shift at δ= 5.32-5.55 ppm (g, -CH) corresponds to the two methine protons of MG_{CO}. The proton attached with the N-atom of urea and urethane groups were

found at δ= 6.87-7.06 ppm (h, -NH) and δ=7.92-7.96 ppm (i, -NH), respectively. However, the proton attached to the N-atom adjacent to the benzene ring of 2-APDS appeared at δ=9.09-9.11 ppm (j, -NH).

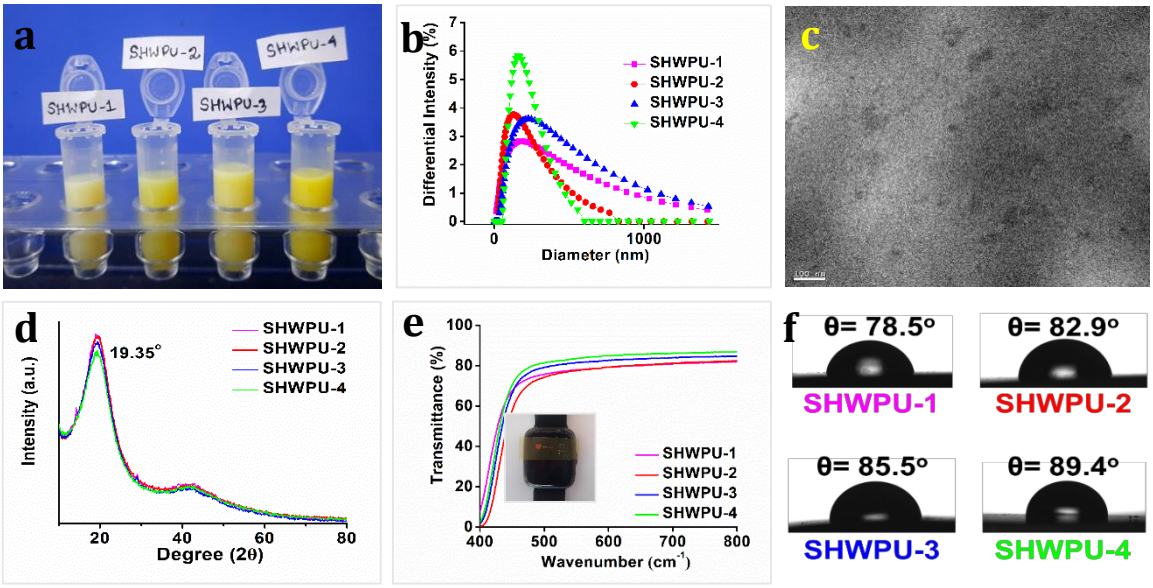

Figure 5.3. (a) Digital images of SHWPUs dispersion keeping in Eppendorf tube, (b) particle size distribution curves, (c) TEM images of SHWPU-2 dispersion (100nm), (d) powder X-ray diffraction (P-XRD) patterns, (e) percentage of transmittance spectra, inset: a small heart is visible through the SHWPU-4 film, and (f) contact angle of SHWPUs film.

The assumed chemical structure of SHWPU-2 was further confirmed from the ^{13}C NMR spectrum as shown in **Figure 5.2 (b)**. A perusal of the ^{13}C spectrum of SHWPU-2 showed that the NMR absorption peaks at δ= 24.54 ppm (a), 25.36 ppm (b), and 35.44 ppm (e) correspond to the β, γ, and α-C atoms concerning the ester group of ε-PCL component. The free methyl C-atoms of IPDI and IPDA were found at δ= 28.27 ppm (c) and δ=33.84 ppm (d). A large peak at 63.93 ppm (f) can be assigned to the C-atom attached to the O-atom of the urethane linkage. Furthermore, the NMR absorption at δ= 156.01 ppm (g) and δ= 173.16 ppm (h) can be accredited to the carbonyl C-atom (C=O) of urethane and ester group originated from various reactants used to prepare SHWPU-2 [5]. **Figure 5.3 (a)** depicted the digital images of stable aqueous dispersions and particle size distributions of various SHWPUs. There is an enhancement of yellowish color with the increment of 2-APDS content. DLS study revealed the average diameters and polydispersity indices of SHWPU-1, SHWPU-2, SHWPU-3, and SHWPU-4 were 267.1 nm and 0.352, 175.4 nm and 0.258, 334.1 nm and 0.317, and 192.2 and 0.193, respectively. Again, the zeta potential (ζ, mV) values of SHWPU dispersion were in the range of -45.9 mV to -69 mV. Furthermore, there is no significant precipitation in all samples after centrifugation at 2500 rpm for 10 min. These results and experiments validated the formation of good nano-emulsions with high

stability for up to 6 months without significant coagulation and interestingly, miniature-shaking results in the original emulsion [6]. TEM images (**Figure 5.3 (c)**, SHWPU-2) also support the same. The crystalline phases of SHWPUs were scrutinized by P-XRD at 2θ =10° - 80°, as shown in **Figure 5.3 (d)**. The pure ε-PCL_{2000} is a semi-crystalline material that exhibited two XRD patterns at 21.4° and 23.8° corresponding to (110) and (200) reflection plans. However, these two peaks disappeared, and a broad peak was found at 19.35° which refers to the development of micro-phase separation (hard phase and soft phase) during polymerization [7]. Also, the peak was only because of the soft segment i.e., PCL moiety. It has been observed that the peak intensity slightly decreases from SHWPU-1 to SHWPU-4 with the increase in hard domains along with 2-APDS content, resulting in more phase separations. As shown in **Figure 5.3 (e),** the transparency of SHWPU-1, SHWPU-2, SHWPU-3, and SHWPU-4 were 81.40%, 82.15%, 84.40%, and 87.04%, respectively. Again, gel permeation chromatography (GPC) study showed that all PU elastomers exhibited satisfactory weight average molecular (M_w) in the range of 54089-94935 $gmol^{-1}$ and polydispersity index (PDI) from 1.462 to 1.57. As shown in **Figure 5.3 (f)**, the water contact angles of SHWPU-1, SHWPU-2, SHWPU-3, and SHWPU-4 were found to be 78.5°, 82.9°, 85.5°, and 89.4°, respectively. Zhang and his coworkers also obtained a similar trend of results [8]. Literature reveals that several factors affect the contact angle of SHWPU films including, the polarity of the polyols, cross-linking density, and content of the emulsifier [9]. In the present study, all composition contains the same amount of polyols and internal emulsifier (DMPA and GECA). Therefore, the change in the trend of the water contact angle of SHWPU films solely depends on the cross-linking density. The P-XRD showed that the crystallinity decreased from SHWPU-1 to SHWPU-4 that refers to the increase in the cross-linking density. In addition, the hard-to-soft segment ratio highly and directly influences the resultant properties of a designed WPU elastomer. Notably, in the present work, the hard segment consists of asymmetric IPDI-IPDA architecture, and higher the amount of hard segment, higher is the phase separation due to the higher degree of crosslinking, and the lower is the crystallinity. Furthermore, the presence of a small percentage of 2-APDS provides a thermodynamic driving force that renders the surface hydrophobic [10].

5.3.2. Thermal analysis of SHWPUs

The thermal deterioration of SHWPUs is a complex multi-step process in which various partial decomposition reactions occur at different temperatures.

Table 5.2. Characteristic parameters of SHWPUs obtained from TGA and DSC analyses.

Sample Code	T_1 (°C)	T_{MAX} (°C)	T_2 (°C)	T_g (°C) (Hard segment)	T_m (°C) (Soft segment)	T_g (°C) (Soft segment)	T_C (°C)
SHWPU-1	252.5	323.2	427.4	32.2	57.2	-6.1	55.2
SHWPU-2	251.6	324.6	433.9	41.6	56.5	-6.0	50.2
SHWPU-3	249.9	322.9	433.5	64.8	56.9	-6.0	50.6
SHWPU-4	248.2	321.2	434.8	68.1	59.6	-6.0	50.6

Several factors affect the thermal degradation of SHWPU which include the presence of hard moiety like benzene ring, the hard-to-soft segments ratio, molecular weight of the polymer, degree of physical or chemical cross-linking, etc. [11]. The results of the thermal studies for SHWPU were demonstrated in **Figure 5.4** and summarized in **Table 5.2**. The thermogravimetric process of SHWPU could be illustrated in three major steps. The first step degradation, T_1= 248.2 - 252.5 °C might be because of the thermal decomposition of 2-APDS to form benzene, sulfur, and other volatile compounds [12]. A major mass loss was found in the second step of degradation, T_{MAX} = 321.2 - 324.6 °C which can be attributed to the deterioration of carbamate groups, urea linkages, ester linkages, and moiety of MG_{CO}. Final step degradation (T_2= 427.4 - 434.8 °C) occurred because of the degradation of thermostable moieties including the benzene ring of 2-APDS and the cycloaliphatic ring of IPDA and IPDI. It has been observed that the thermal stability increases from SHWPU-1 to SHWPU-4 at high temperatures. This increment might be developed because of the gradual increase in the benzene ring structure of 2-APDS. Again, **Figure 5.4 (c)** and **(d)** showed DSC thermograms for SHWPUs. The glass transition temperature (T_g) of the hard segment of SHWPUs, which was determined from the temperature related to the peak in tanδ curves, demonstrated a noticeable increase with the increase of 2-APDS i.e., hard phase. As shown in **Table 5.1**, when the amount of 2-APDS increased from 2.71% to 11.23%), the T_g (hard segment) of the elastomers increased from 32.2 °C to 68.1 °C measured by DSC. Remarkably, all SHWPU

exhibits a broad T_g peak, which may assist in the multi-shape memory effect. The rigid benzene rings of 2-APDS and GECA (with four hydroxyl groups) resist the molecular chain mobility, resulting in high T_g [8].

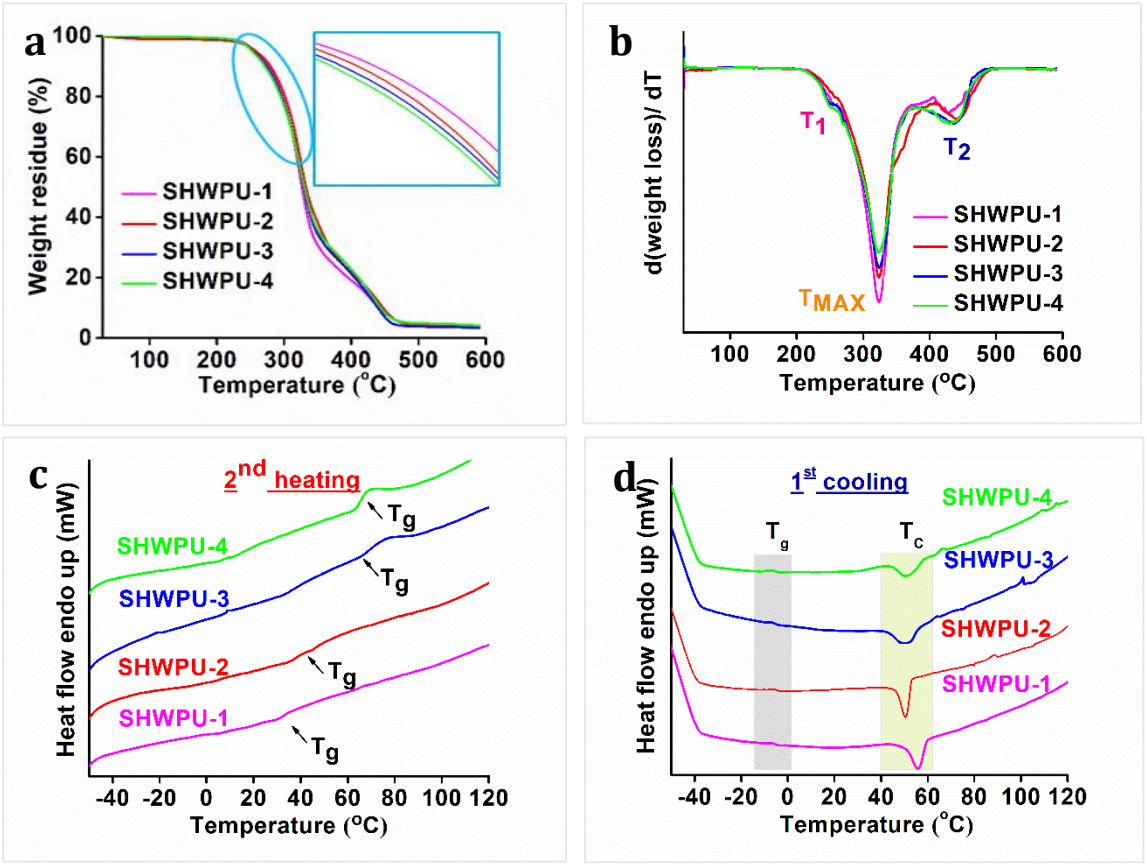

Figure 5.4. (a) TGA thermograms, (b) DTG curves, and (c-d) DSC curves of SHWPU films.

Furthermore, broad melting peaks (T_m, near 56-60 °C) were observed in the first heating cycle. However, these might be overlapped with the glass transition temperature (T_g) of the hard segment in the second heating cycle because of the thermal cross-linking after 1st cycle of heating [13]. Furthermore, due to high rate of cooling in the cooling cycle, growth of nucleation of crystals was difficult. Therefore, the melting peaks are not found in the second heating cycle.

5.3.3. Mechanical properties of SHWPUs

To evaluate the mechanical properties of SHWPU, the stress-strain curves were compared in **Figure 5.5 (a)** and summarized in **Table 5.3**. The mechanical strength and elongation at break of SHWPU-1, SHWPU-2, SHWPU-3, and SHWPU-4 were 16.08 MPa and 2071%, 18.06 MPa and 2007%, 24.56 MPa and 1755%, and 26.23 MPa and 1604%, respectively. So, the elongation at break or stretchability decreases but the tensile strength is augmented with an increase in 2-APDS content. Comparably, the SHWPU-4 exhibited 1.63 times greater strength

than the SHWPU-1 which contains the lowest amount of 2-APDS. This enhancement occurred because of the rigid structure of the benzene rings of 2-APDS, alicyclic rings of IPDI-IPDA, chemical crosslinking for GECA, and strong hydrogen bonding. These results are consistent with the previously reported data [8]. It is familiar that the mechanical properties of an elastomer are highly influenced by several factors such as average molecular weight, hard-to-soft segment ratio, physical-chemical crosslinking, chain entanglement, the presence of rigid moieties in the polymeric chain, and so forth.

Table 5.3. Mechanical properties of the SHWPU films.

Property	SHWPU-1	SHWPU-2	SHWPU-3	SHWPU-4
Tensile strength (MPa)	16.09±1.33	18.06±1.17	24.56±1.34	26.23±1.67
Strain (%)	2071±121	2007±152	1755±144	1604±130
Toughness (MJm^{-3})	188.3	191.9	212.7	216.6
Hardness (Shore A)	33	38	38	38
Scratch hardness (kg)	≥6.5 ±0.25	≥6.5±0.25	≥6.5±0.25	≥6.5±0.25

Remarkably, the toughness value of SHWPU-1, SHWPU-2, SHWPU-3, and SHWPU-4 were found to be 188.3 MJm^{-3}, 191.9 MJm^{-3}, 212.7 MJm^{-3}, and 216.6 MJm^{-3}, respectively, as shown in **Figure 5.5 (b)**. Thus, all SHWPU elastomers exhibit significant mechanical robustness which is a great challenge for a self-healable polymer. Again, to understand the strain hardening i.e., mechanical performance, the stress-strain curve of SHWPU-3 was considered and divided into three characteristic regimes, as demonstrated in **Figure 5.5 (c)**. A slow quasi-linear increment of mechanical strength within a wide range of strain was observed in Regime 1 which can be attributed to the molecular chain rearrangement, disentanglement and alignment of soft domains, and development of aggregation state. This conjecture is supported by the gradual decrement of transparency and appearance of the minute whitish spot on SHWPU-3 film as it was stretched to 3X of the original length (**Figure 5.5 (d)**). Again, Regime 2 and Regime 3 showed an intermediate and sharp quasi-linear increase in strength, respectively. At these regimes, the film becomes more whitish. This can be explained as the development of a specific phase with a distinct refractive index during large deformations via the crystallization of soft domains between associative hard segments [14]. This phenomenon is analogous to the strain-induced crystallization (SIC) of natural

rubber that assists in the improvement of mechanical strength. Eventually, the toughness is directly associated with the energy dissipation capacity and hence tensile strength and stretchability of the elastomer. Although, these two properties are contradictory to each other, here, an optimum result was obtained by optimizing chemical compositions, precisely.

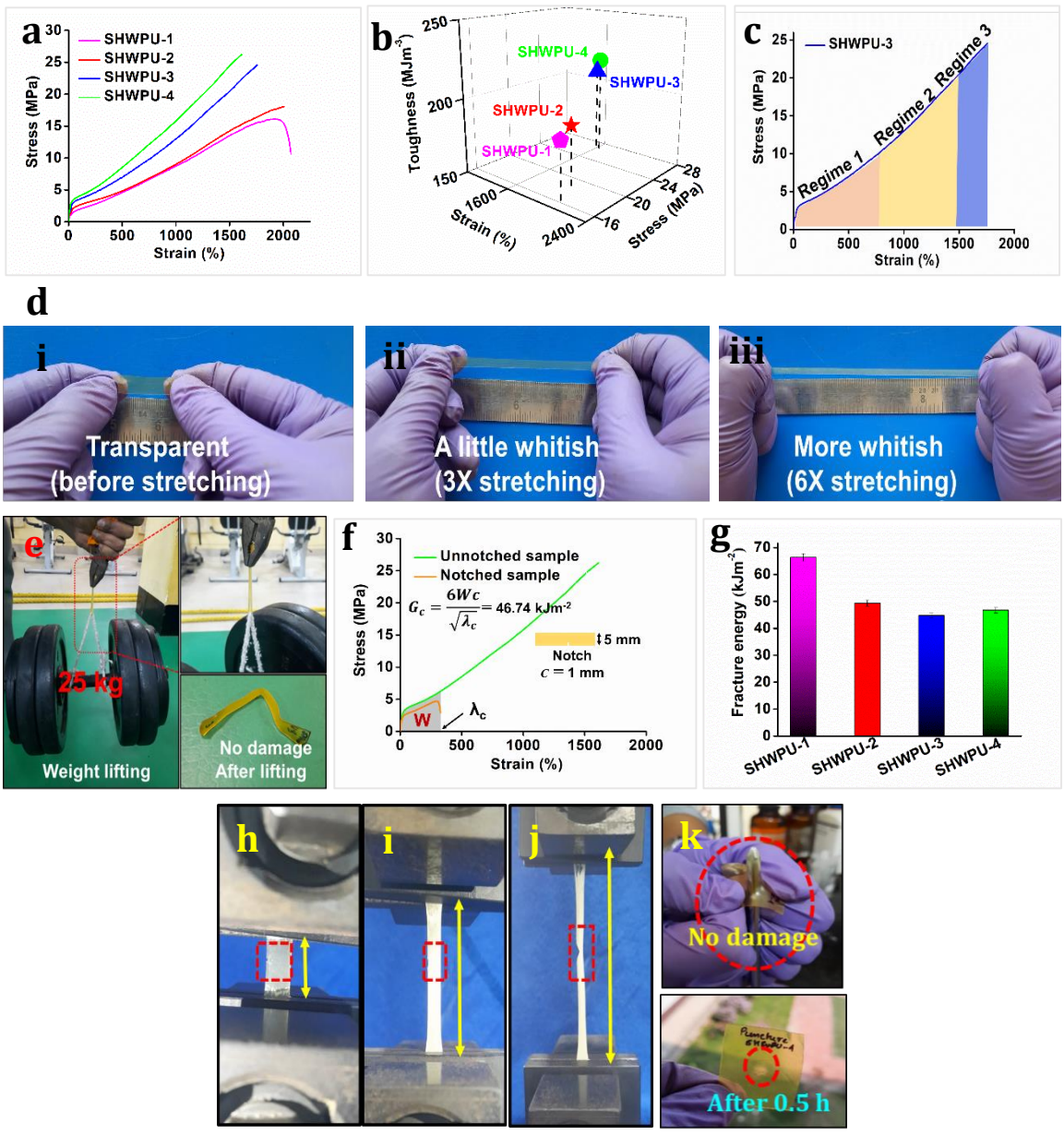

Figure 5.5. (a) Stress-strain profiles, (b) 3D curve of toughness of SHWPU films, (c) stress–strain profile of the SHWPU-3 elastomer divided into three regimes, (d) digital photos showing the whitening process of SHWPU-3 with increase in strain (%), and (MJm^{-3}), maximum tensile stress (MPa), and strain (%) of all SHWPU films, (e) lifting a dumbbell of 25 kg using SHWPU-3 (0.466 g), (f) stress-strain curve of un-notched and notched (1 mm) SHWPU-4 film, (g) fracture energy of SHWPUs determined using Greensmith's method, (h-j) digital photos of fracture test (SHWPU-2), and (k) puncture test of SHWPU-4.

Outstandingly, an SHWPU-3 sample (0.466 g, length 50 mm, width 8 mm, and thickness 1.02 mm) can lift a dumbbell of 25 kg, which is 53648 times heavier than its weight

without any crack, as shown in **Figure 5.5 (e)**. This is clear evidence of the excellent mechanical robustness of the developed SHWPUs. Moreover, the fracture energies were measured by Greensmith's method to investigate quantitative the crack tolerance of SHWPUs [15]. **Figure 5.5. (f-j)** illustrated the details of the fracture energy of SHWPUs. Furthermore, we tried to puncture an SHWPU-4 film (thickness ~ 0.5 mm) but failed to puncture it after three consecutive attempts. **Figure 5.5 (k)** demonstrated the puncture resistance of the tested film. In other words, these tests also support the extreme toughness of the developed elastomers.

Table 5.4. Mechanical data of the SHWPU films after self-healing at 110±5 ℃for 2h.

Sample code	Tensile strength (MPa)	Healing efficiency (%)	Elongation at break (%)	Healing efficiency (%)
SHWPU-1	11.29±0.37	70.22	1375±107	66.39
SHWPU-2	12.92±0.61	71.54	1543±113	87.92
SHWPU-3	18.93±0.44	77.08	1515±121	75.48
SHWPU-4	20.97±0.36	79.95	1308±115	81.54

5.3.4. Self-healing, shape-memory, and reprocessable performances of SHWPUs

To evaluate quantitative healing efficiency, all SHWPU films (50 mm × 10mm × 0.8 mm) were cut into two pieces using a sharp blade, rejoin, and then placed in a convection oven at 110±5 ℃ for 2 h for the healing treatment. Here, the self-healing efficiency was defined as the percentage of recovery of tensile strength after healing. The results were summarized in **Table 5.4** and demonstrated in **Figures 5.6**. The remarkably good healing efficiency and high tensile strength were achieved by introducing dynamic hard domains (2-APDS), GECA, and asymmetric architecture (IPDI-IPDA) into the hard domains. In SHWPUs, the healing ability originated from two prime sources, i) reversible physical interactions (hydrogen bonding) and ii) metathesis of dynamic disulfide bond which is further assisted by the shape memory attribute, as shown in **Scheme 5.1 (b)** and **5.6 (a)**. Firstly, the multiple hydrogen bonds (both weak and strong) developed between the urea-urea, urea-carbamate, and carbamate-carbamate groups. The asymmetric IPDI-IPDA moiety not only generates strong multiple hydrogen bonding but also enables molecular chain mobility by forming loosely

packed hard domains, retaining excellent mechanical properties. This moiety is analogous to 1,4-cyclohexanediemthanol (CHDM) which is commonly used to prepare low polyester with low viscosity without affecting the mechanical strength of the final product [16-17].

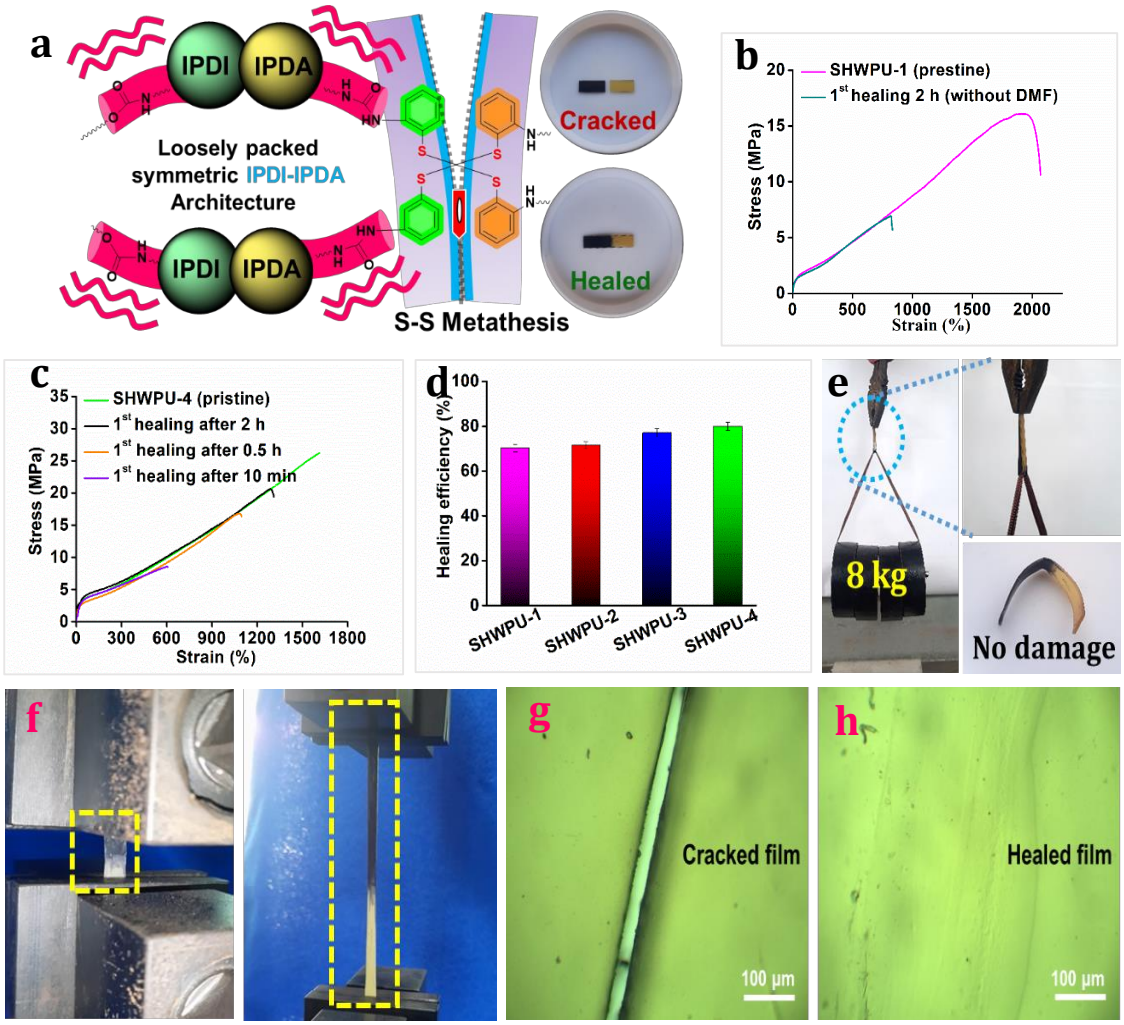

Figure 5.6. (a) Graphical illustration of the healing process, stress-strain profiles of (b) pristine and healed SHWPU-1 film at 140±5 °C for 2h without DMF, (c) pristine and healed SHWPU-4 films heated at 110±5 °C for different times (2h, 0.5h, and 10 min) with DMF, (d) healing efficiency (%) of SHWPUs, (e) weight lifting test (8 kg), (f) stretching test for SHWPU-3 after healing, and (g-h) optical microscopic images before and after healing (scale = 100 µm).

Secondly, most importantly, lower S-S bond dissociation energy (60 kcal mol^{-1}) and disulfide metathesis reaction greatly advance the healing process and diminishes healing time [18]. Additionally, the shape memory effect also promoted the self-healing ability via shape recovery [8]. Literature disclosed that the healing mechanism consists of five major steps: i) surface rearrangement, ii) surface approach, iii) wetting, iv) diffusion, and v) randomization [19]. In the present study, the randomization is driven by dynamic disulfide metathesis. Initially, in this study, we tried to heal the damaged film by applying heat only. But the healing efficiency of SHWPU-4 obtained was only 43.13% at 140 °C for 1h, as shown

in **Figure 5.6 (b)**. Later on, we used a trace amount of solvent (0.1-0.2 µL of DMF) to rejoin and heal the cracked films. As expected, the healing efficiency was improved up to 79.95% (SHWPU-4), as shown in **Figures 5.6 (c)** and **(d)**. Importantly, the use of trace solvents might not misbalance the environmental stability and not causes a dissolution effect that needs a high amount of solvent. Furthermore, the structural integrity (structural deformation and uniformity) of the films did not lose because of the used solvent as shown in **Figure 5.6 (a)** (black-yellow film). Results showed that the healing efficiency of SHWPU-4 is higher than that of SHWPU-1 (**Table 5.4**). This can be illustrated due to the high disulfide bond content in the SHWPU-4 matrix [20]. To further investigate the self-healing ability of SHWPUs, SHWPU-4 was considered as the example and healed at 110±5 ℃ at different times, as represented in **Figure 5.6 (c)**. This can be accredited to the increase in the intensity of diffusion and randomization i.e., the disulfide exchange reaction in the polymeric films with time that is highly recommended for the development of a polymeric network after the damage [8].

The qualitative investigation of the healing ability of SHWPU was done by weight-lifting test and stretching test as shown in **Figure 5.6 (e)** and **(f)**. Most interestingly, the healed SHWPU-3 film (length 60 mm × width 8 mm × thickness 0.8 mm) can successfully lift a weight of 8 kg. This test ensured the excellent healing ability of the developed robust SHWPU elastomers. To the best of our knowledge, there is no article so far published that has shown the lifting of that much weight by the healed film. Conclusively, the optical microscopic images (**Figure 5.6 (g)** and **(h**) of the cracked and the healed film also support the same.

Table 5.5. The shape memory effect of SHWPU films.

Parameters	**SHWPU-1**	**SHWPU-2**	**SHWPU-3**	**SHWPU-4**
Shape fixity (%)	95.3	93.7	91.3	90.2
Shape recovery (%)	97.4	96.8	89.3	88.4
Shape recovery under heat (T_g+ 20 ℃, water) (s)	50±5	80±5	120±5	120±5

Further investigation revealed that all SHWPUs exhibited excellent shape memory in warm water at 80 °C within 3 min, as shown in **Figure 5.7 (a).** Three parameters, namely, shape fixity (%), shape recovery (%), and recovery time (s) were quantified according to equations **Eq.5.1** and **Eq. 5.2**, and furnished in **Table 5.5**. The shape memory performance of SHWPUs is greatly affected by the presence of crystalline segments and the crosslinking density of hard domains i.e., micro-phase separation.

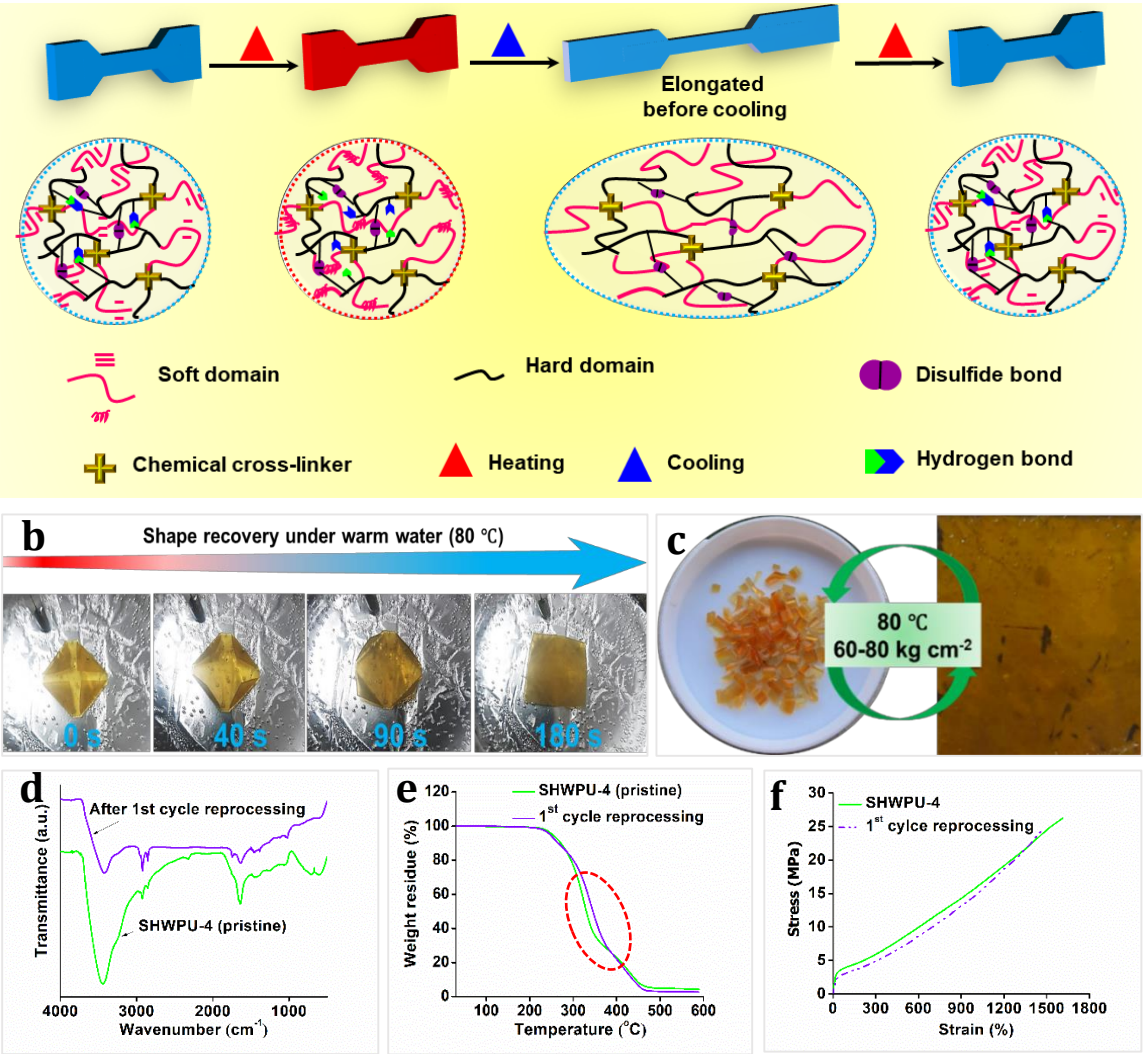

Figure 5.7. (a) Plausible mechanism of the shape recovery process, (b) shape recovery test underwater at 80 °C, (c) reprocessing of SHWPU-4 films at 80 °C under a pressure of 60-80 kg cm^{-2}, (d) FTIR spectra, (e) TGA thermograms, and (f) stress-strain profile of the pristine and reprocessed SHWPU-4 film.

The literature explains that the shape memory ability of material is consisting of two primary phenomena: i) "memory" of a stress-free permanent shape and ii) "programming or fixing" of a temporary shape via the heating-deformation-cooling process [21]. The memory of the permanent shape is controlled by the reversible phase (physical or chemical crosslinking), while shape fixing (fixation phase) is accomplished by kinetic trapping of a

deformed and stressed shape by crystallization, vitrification, and plastic deformation [22-23]. In this study, the SHWPU films were heated at T_g+20 ℃ (hard segment) to develop the Brownian movement of the molecular chains. At this fragile moment, the entropy of the polymeric system is maximum, so a temporary shape was fixed via immediate freezing (-5 ℃). Here, the semi-crystalline plays a great role in the fixation phase. On the other hand, the reversible phase originated from hard segments i.e., a combination of 2-APDS, IPDI-IPDA, MG_{CO}, and GECA, which help in the shape recovery at T_g+20 ℃. Noticeably, as the percentage of 2-APDS increased from 2.7% to 11.22%, the shape fixity (R_f, %) decreased from 95.3% to 90.2% which is due to an increased percentage of the hard segment and decrease in the crystallinity [24-25]. Again, the shape recovery (R_r, %) of SHWPU-1 and SHWPU-2 is greater than that of SHWPU-3 and SHWPU-4. This dramatic decrease in the R_r value can be accredited to the gradual increment of chain mobility with high content of disulfide bond. Importantly, the shape memory effect can be utilized for developing artificial muscle which was tested in this report.

Since all the SHWPU contains disulfide bonds and multiple-hydrogen bonds that can be destroyed and re-created unlimited times through free radical generation and recombination. So, these elastomers exhibit good reprocessable attributes along with robust mechanical strength, self-healing, and shape memory properties. By considering SHWPU-4 as an example, the physical reprocessing was done as follows. Firstly, used films were cut into small specimens (~ 4 mm^2) and placed inside two metallic plates (mold). Then, the plate was subject to the compression molding machine at 80 ℃ under 60-80 kg cm^{-2} pressure for approximately 1.5 h and finally, allowed to cool down to 25-30 ℃. As this process does not require additional solvent (s) or catalyst, it is extremely useful for industrial applications [8]. However, IPDI-IPDA based modified hard domains are insensitive to moderately high temperature. The mechanical properties, thermal stability, and structural change (FTIR study) of the reprocessed film were evaluated and compared as shown in **Figure 5.7. (c-f)**. But significant change was observed. Remarkably, SHWPU-4 exhibited better thermal stability than the pristine elastomer after reprocessing. However, tensile strength and elongation at breaks were found to be 24.66 MPa and 1477%. This is because of the blistering formed during the compression process which perturbed the uniformity of the films. But, most importantly, this result is highly acceptable for the development of sustainable smart materials.

5.3.5. Hemocompatibility assay of SHWPU films

Here, we have set out to fabricate clinically relevant materials for stent, conduits, and sutures which demands negligible platelet adhesion and activation. This nature would prevent the chances of thrombogenesis as well as atherosclerosis in vivo. SHWPU was assessed for its platelet adhesion and platelet activation properties with the collagen-coated surfaces as positive controls. SHWPU films demonstrated minimal platelet adhesion in contrast to the positive control. The cytoskeletal staining of rhodamine-phalloidin was carried out and the platelets stained with red fluorescence are visible in the micrographs (**Figure 5.8 (a)**). Thereafter the SHWPU-coated and positive control surfaces were used to assess the activation potential of the adhered platelets.

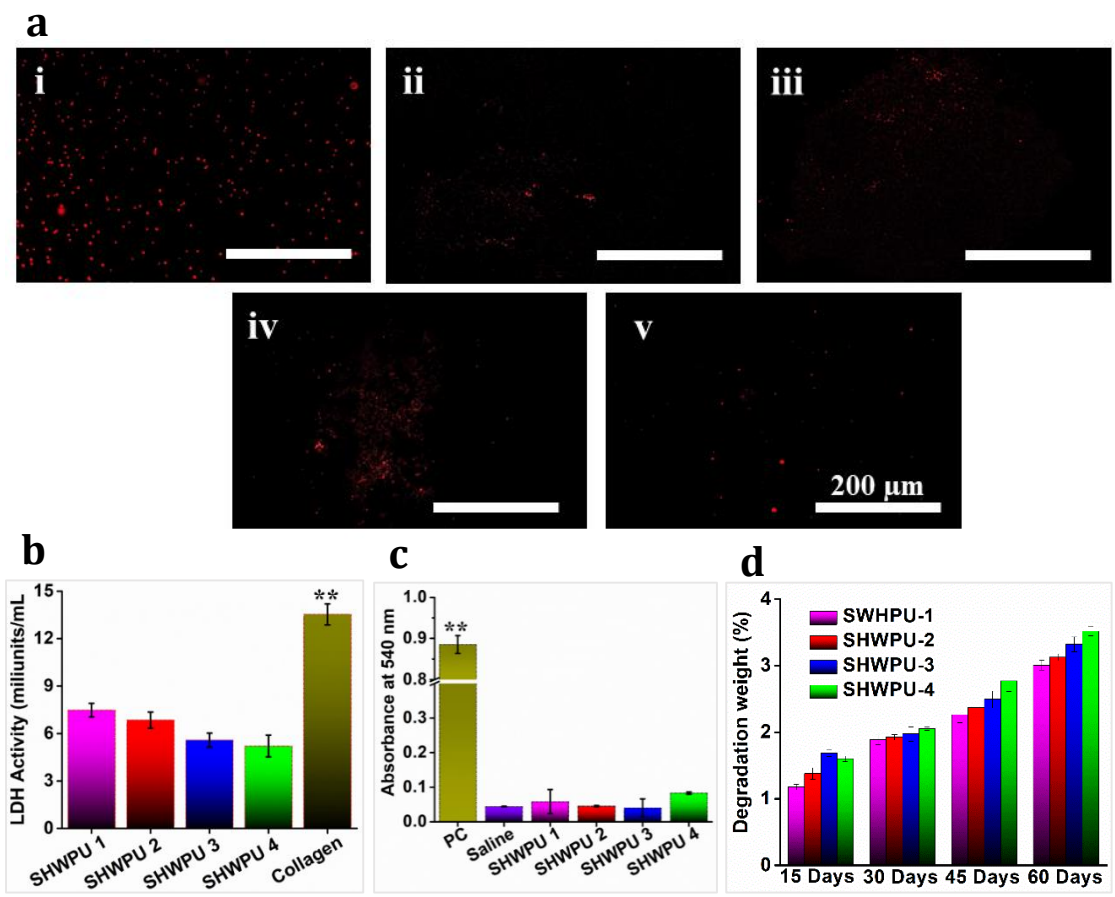

Figure 5.8. (a) Representative rhodamine-phalloidin stained micrographs of platelets adhere on (i) collagen coated surface, (ii) SHWPU-1, (iii) SHWPU-2, (iv) SHWPU-3, and (v) SHWPU-4, (b) LDH activity of the platelets adhered on the various SHWPU surfaces as compared with collagen as the positive control, (c) RBC lysis caused by PC (positive control) (20% Triton-X 100), saline (150 mM NaCl) and various SHWPU surfaces measured optically, and (d) degradation of various films on days 15, 30, 45 and 60 days incubated in 0.1M PBS expressed as weight percentage degraded. (n=3, **p≤0.001) (scale bar: 200 µm).

LDH activity of the adhered platelets was measured using a kit to determine their activation following our previous methodology [26]. The platelets that were adhered in the positive control samples i.e., collagen-coated surfaces showed significantly higher LDH

activity ($p \leq 0.01$) in contrast to the SHWPU films. The SHWPU films which showed very low LDH activity of the platelets adhered to the same (**Figure 5.8 (b)**). The LDH activity in all the groups of the SHWPU films was found to be similar and all were significantly less than the collagen-coated surface. Hence, they could be dubbed anti-thrombogenic. Further analysis of SHWPU material-based stents, conduits, or constructs in vivo would be essential for the confirmation of this nature. Blood compatibility was also assessed for the SHWPU samples using an RBC lysis assay. The SHWPU disks were found to not lyse the RBCs during the incubation. Also, the lysis produced by 20% Triton X-100 was found to be significantly higher ($p \leq 0.01$) than that of the SHWPU samples (**Figure 5.8 (c)**). RBC lysis response of the SHWPU disk variants was found to closely mimic the effect of 150 mM NaCl buffer, i.e., the negative control. The significantly low RBC lysis, minimal platelet adhesion as well as significantly low platelet activation in vitro reiterate our hypothesis of overall hemocompatibility of the various SHWPU disks. These materials could find potential use in many biomedical applications such as the development of stents, conduits, sutures, and scaffold materials.

5.3.6. *In vitro degradation assessment*

For the long-standing stability of biomedical materials, their degradability is crucial in determining their applicability. The SHWPU films were incubated in saline solution for 60 days, and they underwent slow degradation. Weight loss of ~ 3% was found in all of the SHWPU disks for 60 days (**Figure 5.8 (d)**). This is in concurrence with the results of previously observed PU composite materials [27]. This rate of degradation would potentially enable long-term in vivo stability. Slower degradation is ideal for long-standing constructs such as stents, sutures as well as conduits. These SHWPUs could be further introduced in vivo and could be studied for the subsequent interaction with other bodily fluids and tissues containing various enzymes and cells. This interaction with the exposed materials to other physicochemical conditions and hence be the determining factor of the actual degradability of various SHWPU material forms.

5.3.7. *In vitro* cell viability and proliferation

Alamar blue reduction has been directly correlated with the enhanced metabolic activity of cells as well as their proliferation [27]. The SHWPU disks were seeded with HDFs, and they were found to support the proliferation of the same. HDFs could proliferate >1.25 times on all the SHWPU disk variants for 7 days. The proliferation was found to be the highest in SHWPU-4 (>1.35 times) disks and the lowest in SHWPU-1 (~1.25 times) disks amongst the SHWPU disks after 7 days of culture (**Figure 5.9 (a)**). While this rate of proliferation was

significantly lower than the TCP (Tissue Culture Plate) control (>2 times, $p \leq 0.01$) but the cells were found to be metabolically active and underwent mild proliferation in vitro (**Figure 5.9 (b)**). Post in vitro culture of 7 days, live/dead assay was performed on the HDFs for assessment of their viability and morphological traits when seeded on the various SHWPU disks. The HDFs were found to be viable on the TCP with an adhered and spread morphology (**Figure 5.9 (c)**). Concurrently, SHWPU surfaces showed HDFs in their rounded and partially spread morphology along with the formation of aggregates.

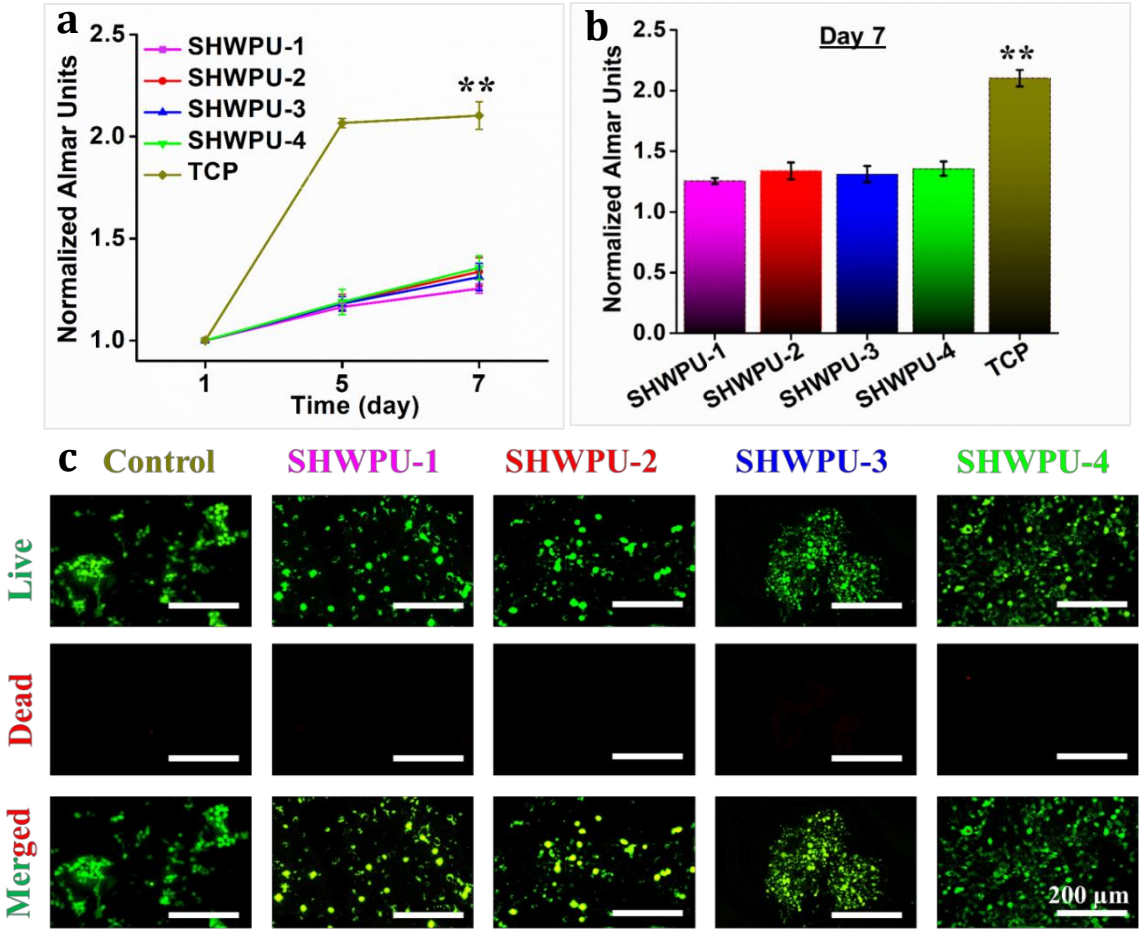

Figure 5.9. (a) Alamar blue-based cellular proliferation of HDF seeded on various SHWPU surfaces and control (TCP), (b) reduced Alamar units on day 7 depicting the variation in a proliferation of HDF on various surfaces. (n=4, **p≤0.01), and (c) representative micrographs showing live-dead imaging after 7 days of incubation in control, SHWPU-1, SHWPU-2, SHWPU-3, and SHWPU-4 (scale bar: 200 µm).

Cellular viability and proliferation studies suggested the in vitro biocompatibility of the various SHWPU materials as well as corroborated their ability to support cellular adhesion as well as proliferation. In vivo, the compatibility of these developed materials could be evaluated in the future in various forms such as self-tightening sutures, self-forming conduits, or stent materials.

5.3.8. SHWPU elastomer as artificial muscle and 3D printable ink

As the developed virgin SHWPU elastomer exhibited excellent shape memory performance, the energy storing and releasing of this elastomer had a future in the area of artificial muscles. As shown in **Figures 5.10 (a-f)**, the elongated SHWPU-1 film could vertically lift a 100 g load, successfully, which is 251.19 times its weight upon exposure to heating for 120 s. This facilitates its usability as a soft artificial muscle. Wang and his co-workers obtained a similar result for their products [28]. Furthermore, 3D printing of partially solidified gelatin/SHWPU-2 (**Table 5.6**) ink was performed to judge its suitability in biomedical scaffold applications.

Table 5.6. The optimized machine parameters and ink compositions.

Parameter/composition	Dimension/percentage
Scaffold dimension	3.5 cm X 3.5 cm X 2 cm
Layer height	0.25 mm
Shell thickness	0.40 mm
Fill density	15 percent
Flow rate	20 percent
Printing speed	3.5 mm/second
Ink 1(1:0.5)	Gelatin (20 % wt/v) /SHWPU-2
Ink 2 (1:0.3)	Gelatin (20 % wt/v) /SHWPU-2

Due to difficulties in the ink solidification caused by an increased amount of SHWPU-2, the printed Ink 1 based scaffold layers were not found to be dimensionally stable. Even after drying, the majority of the scaffold's pores were still found to be covered by spilled materials. However, the printed scaffold layers were found to be dimensionally stable up to 6 layers after reducing the amount of SHWPU-2 in the ink formulation from 1:0.5 to 1:0.3 (**Figure 5.10 (g)** and **(h)**). Thus, Ink 2 formulation was found to be printable as a scaffold. But ink consolidation at the cross-sectional locations and adding more layers than 6 at a level were found to be difficult. The fabricated scaffolds were shown to be dimensionally stable upon drying in a hot air oven for 48 h at 50 ℃. However, as layer height grew result led to decreased porosity (**Figure 5.10 (n-r)**). At room temperature, 3D bio-printed

gelatin/SHWPU-2 ink demonstrated good printability at a certain level of layers. Gelatin/SHWPU-2 scaffolds offer substantial possibilities in tissue engineering as SHWPU-2 showed biocompatible with HDF cells and gelatin has excellent biocompatibility and is widely used in biomedical fields [29-30]. Increasing the scaffold layer height resulted in ink accommodation at cross-sectional locations, though up to 6 layers could be adequately printed (**Figure 5.10 (r)**). The strength of the scaffold structure of gelatin/SHWPU-2 ink can be modified by adjusting the gelatin/SHWPU-2 weight percentage ratio.

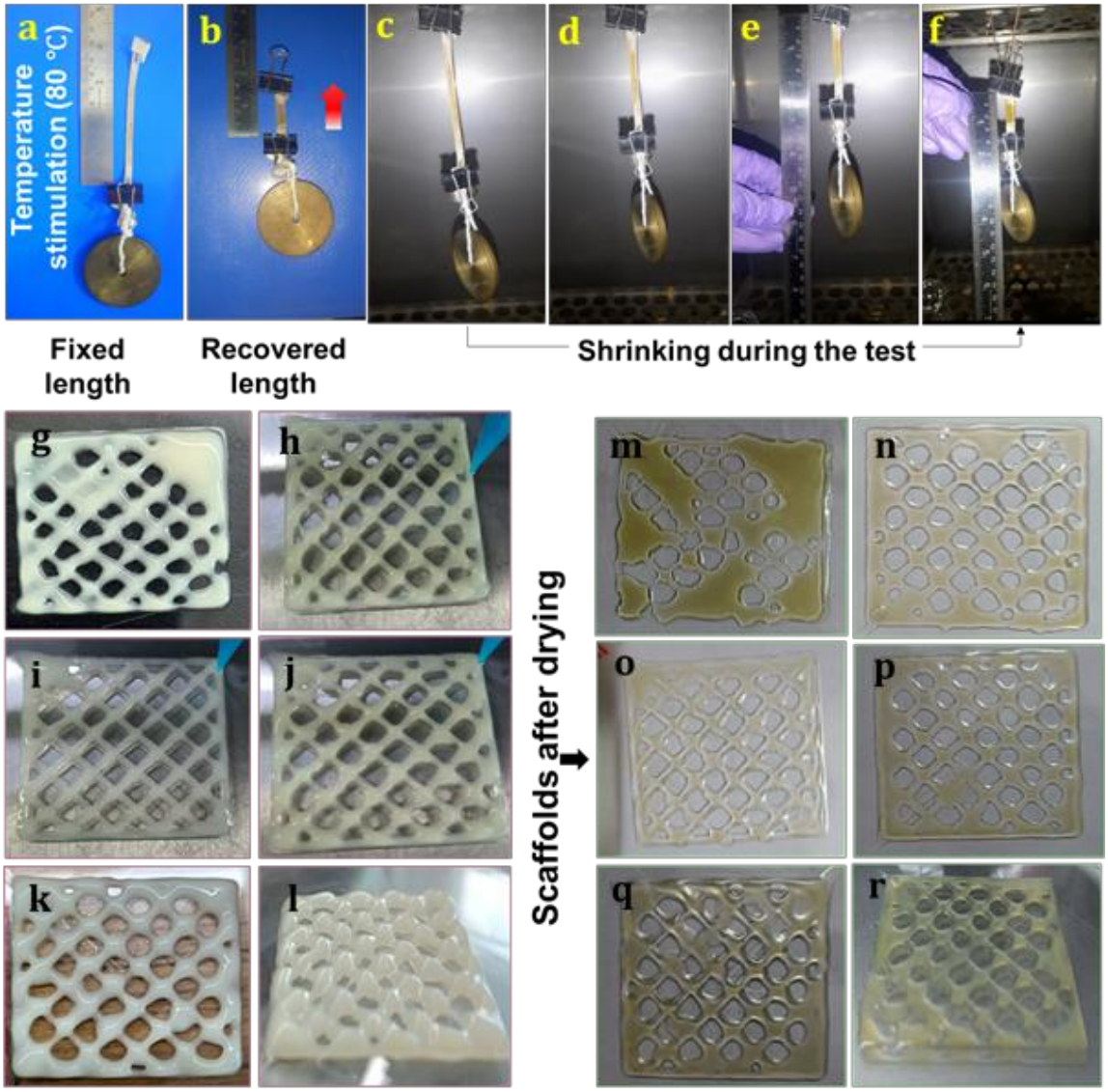

Figure 5.10. (a-b) 'Artificial muscle' contraction stimulate by temperature (80 ℃), (c-f) digital images of various steps during lifting a weight of 100 gm at 80 ℃ for 120 s, scaffold before drying, (g) gelatin (20 % wt/v) /SHWPU-2 (1:0.5), (h) gelatin (20 % wt/v) /SHWPU-2 (1:0.3), (i, j & k) two, four, and six layers of gelatin (20 % wt/v) /SHWPU-2 (1:0.3), (l) side view of six-layered gelatin (20 % wt/v) /SHWPU-2 (1:0.3), and (m-r) scaffold after drying at 50 ℃ for 48 h.

The gelatin/SHWPU-2 ink system demonstrated a technique for creating shape memory properties-based scaffolds for medical applications. The gelatin/SHWPU-2 ink-

printed scaffolds exhibited good dimensional stability and several layers can be enhanced by tuning the temperature of ink, bed (platform), and ambient.

5.3.9. Biodegradation of SHWPUs

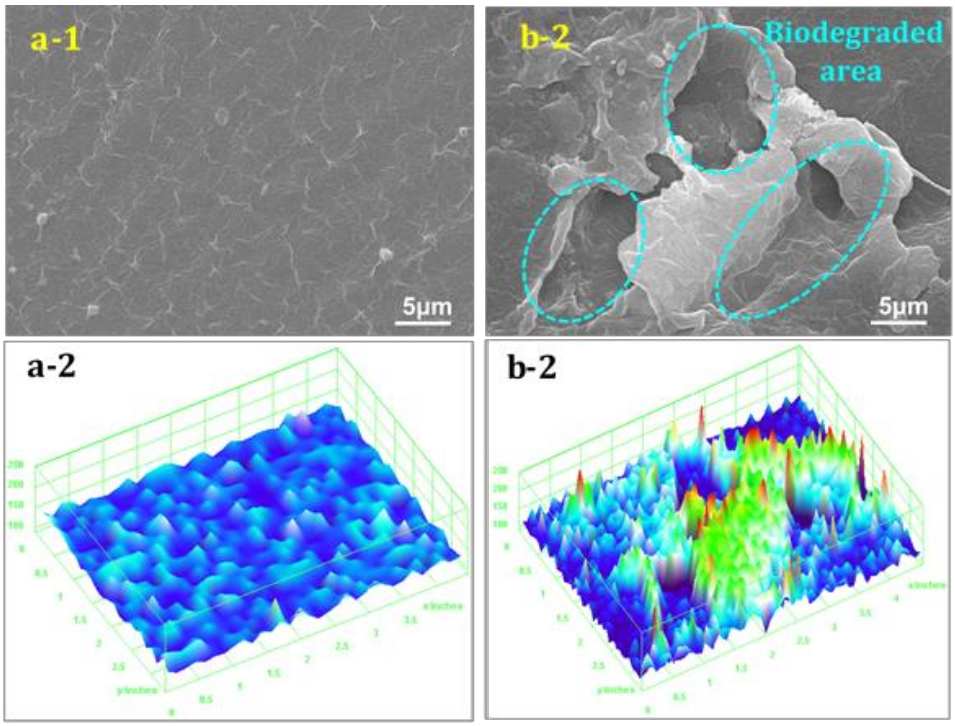

Figure 5.11. SEM images of (a-1) un-degraded and (b-1), degraded SHWPU-4 film and (a-2 and b-2) surface 3D plots of the corresponding SEM images obtained from ImageJ software.

The biodegradability nature of the prepared films was scrutinized by burying them in an open atmospheric soil and allowed to come across various seasonal weather conditions for 60 days. From the SEM images (**Figure 5.11**), it can be seen that the degraded film (SHWPU-4) contains heterogeneous holes and cracks viz. it is bumpier than un-degraded film.

Table 5.7. Weight loss percentage after 2 months of soil burial test.

Sample code	Initial weight (g)	Final weight (g)	Weight loss (%)
SHWPU-1	0.05683	0.05456	3.99%
SHWPU-2	0.05868	0.05675	3.28%
SHWPU-3	0.05839	0.05715	2.12%
SHWPU-4	0.07252	0.07057	2.69%

For better understanding and visualization, SEM images were converted to 3D surfaces using ImageJ software as shown in **Figures 5.11 (a-2)** and **5.11 (b-2)**. The development of surface roughness indicates the bacterial attack on the suitable linkages, e.g., easily hydrolysable ester moiety of SHWPU. The most common bacteria such as *B. subtilis* (gram-positive) can easily attack the polar hydrolysable linkages [31]. Generally, the biodegradation mechanism involves four important steps, namely, diffusion of the water molecule, hydrolysis of ester groups, solubilization, and bacterial attack on the film for the transformation into water, CO_2, and humus [32]. Furthermore, the weight loss percentage calculated after the test confirmed the bacterial degradation of SHWPU-4 films (**Table 5.7**). Thus, the developed elastomers are not only show good performances but also eco-friendly.

5.4 Conclusion

In conclusion, a series of robust self-healable WPUs (SHWPUs) was synthesized which exhibited good healing efficiency, shape recovery, excellent mechanical strength, high elongation at break, outstanding toughness, high fracture energy, reprocessability, and most importantly, biocompatibility, and biodegradability. The developed SHWPU-3 material is so tough that a dumbbell of 25 kg, which is 53648 times heavier than the weight of film, can be successfully lifted without any crack. This maneuver was accomplished via an influential strategy that is based on the triple synergistic effect of 'dynamic hard domain (2-APDS)', 'asymmetric IPDI-IPDA architecture', and 'SME'. The loosely packed IPDI-IPDA moieties and SME encourages the reversible S-S metathesis reactions that resulted in high healing efficiency and mechanical strength simultaneously in the SHWPU elastomer. Concurrently, the semi-crystalline ε-PCL_{2000} moiety induces shape recovery that is further promoted by the GECA. Most essentially, platelet adhesion study, LDH activity, erythrocyte or RBC lysis, cellular viability (live/dead) assay, and cell proliferation (Alamar blue) assay using HDFs seeded on the SHWPU elastomer, confirmed the biocompatibility. The 'artificial muscle' contraction test revealed that an SHWPU-1 film (0. 39811 gm) could vertically and successfully lift a 100 g load which is 251.19 times heavier than its weight under ambient conditions. Furthermore, 3D printability was investigated by the fabrication of gelatin/SHWPU-2 ink. Results showed that up to 6 layers could be adequately printed which indicates its applicability as a bone scaffold. Therefore, the SHWPU elastomer can be considered as an advanced material with smart attributes and environmental benign-ness.

References

[1] An, Z. W., Xue, R., Ye, K., Zhao, H., Liu, Y., Li, P., Chen, Z. M., Huang, C. X. and Hu, G. H. Recent advances in self-healing polyurethane based on dynamic covalent bonds combined with other self-healing methods. *Nanoscale*, 15(14):6505-6520, 2023.

[2] Wang, Z., An, G., Zhu, Y., Liu, X., Chen, Y., Wu, H., Wang, Y., Shi, X. and Mao, C. 3D-printable self-healing and mechanically reinforced hydrogels with host–guest non-covalent interactions integrated into covalently linked networks. *Materials Horizons*, 6(4):733-742, 2019.

[3] Wang, S. and Urban, M. W. Self-healing polymers. *Nature Reviews Materials*, 5(8):562-583, 2020.

[4] Liu, Z., Guo, W., Wang, W., Guo, Z., Yao, L., Xue, Y., Liu, Q. and Zhang, Q. Healable strain sensor based on tough and eco-friendly biomimetic supramolecular waterborne polyurethane. *ACS Applied Materials & Interfaces*, 14(4):6016-6027, 2022.

[5] Wang, M., Hu, J., Ou, Y., He, X., Wang, Y., Zou, C., Jiang, Y., Luo, F., Lu, D., Li, Z. and Li, J. Shape-recoverable hyaluronic acid–waterborne polyurethane hybrid cryogel accelerates hemostasis and wound healing. *ACS Applied Materials & Interfaces*, 14(15):17093-17108, 2022.

[6] Delmas, T., Piraux, H., Couffin, A. C., Texier, I., Vinet, F., Poulin, P., Cates, M. E. and Bibette, J. How to prepare and stabilize very small nanoemulsions. *Langmuir*, 27(5):1683-1692, 2011.

[7] Cheng, D., Wei, P., Zhang, L. and Cai, J. New approach for the fabrication of carboxymethyl cellulose nanofibrils and the reinforcement effect in water-borne polyurethane. *ACS Sustainable Chemistry & Engineering*, 7(13):11850-11860, 2019.

[8] Zhang, C., Liang, H., Liang, D., Lin, Z., Chen, Q., Feng, P. and Wang, Q. Renewable castor-oil-based waterborne polyurethane networks: simultaneously showing high strength, self-healing, processability and tunable multishape memory. *Angewandte Chemie International Edition*, 60(8):4289-4299, 2021.

[9] Yu, F., Cao, L., Meng, Z., Lin, N. and Liu, X. Y. Crosslinked waterborne polyurethane with high waterproof performance. *Polymer Chemistry*, 7(23):3913-3922, 2016.

[10] Shan, S., Wu, X., Lin, Y. and Zhang, A. Tough, self-healing, recyclable bottlebrush polyurethane elastomer with a skin-like strain-adaptive-strengthening property. *ACS Applied Polymer Materials*, 4(10):7554-7563, 2022.

[11] Qu, Q., He, J., Da, Y., Zhu, M., Liu, Y., Li, X., Tian, X. and Wang, H. High toughness polyurethane toward artificial muscles, tuned by mixing dynamic hard domains. *Macromolecules*, 54(17):8243-8254, 2021.

[12] Chattopadhyay, D. K. and Webster, D. C. Thermal stability and flame retardancy of polyurethanes. *Progress in Polymer Science*, 34(10):1068-1133, 2009.

[13] Hu, J., Peng, K., Guo, J., Shan, D., Kim, G. B., Li, Q., Gerhard, E., Zhu, L., Tu, W., Lv, W. and Hickner, M. A. Click cross-linking-improved waterborne polymers for environment-friendly coatings and adhesives. *ACS Applied Materials & Interfaces*, 8(27):17499-17510, 2016.

[14] Li, Y., Li, W., Sun, A., Jing, M., Liu, X., Wei, L., Wu, K. and Fu, Q. A self-reinforcing and self-healing elastomer with high strength, unprecedented toughness and room-temperature reparability. *Materials Horizons*, 8(1):267-275, 2021.

[15] Greensmith, H. W. Rupture of rubber. X. The change in stored energy on making a small cut in a test piece held in simple extension. *Journal of Applied Polymer Science*, 7(3):993-1002, 1963.

[16] Yoon, W. J., Hwang, S. Y., Koo, J. M., Lee, Y. J., Lee, S. U. and Im, S. S. Synthesis and characteristics of a biobased high-T_g terpolyester of isosorbide, ethylene glycol, and 1, 4-cyclohexane dimethanol: Effect of ethylene glycol as a chain linker on polymerization. *Macromolecules*, 46(18):7219-7231, 2013.

[17] Park, S. A., Choi, J., Ju, S., Jegal, J., Lee, K. M., Hwang, S. Y., Oh, D. X. and Park, J. Copolycarbonates of bio-based rigid isosorbide and flexible 1, 4-cyclohexanedimethanol: Merits over bisphenol-A based polycarbonates. *Polymer*, 116:153-159, 2017.

[18] Guo, H., Han, Y., Zhao, W., Yang, J. and Zhang, L. Universally autonomous self-healing elastomer with high stretchability. *Nature Communications*, 11(1):2037, 2020.

[19] Kim, S. M., Jeon, H., Shin, S. H., Park, S. A., Jegal, J., Hwang, S. Y., Oh, D. X. and Park, J. Superior toughness and fast self-healing at room temperature engineered by transparent elastomers. *Advanced Materials*, 30(1):1705145., 2018.

[20] Jing, T., Heng, X., Guifeng, X., Ling, C., Pingyun, L. and Xiaode, G. Highly stretchable, high efficiency room temperature self-healing polyurethane adhesive based on hydrogen bonds–applicable to solid rocket propellants. *Polymer Chemistry*, 12(31):4532-4545, 2021.

[21] Lendlein, A. and Kelch, S. Shape-memory polymers. *Angewandte Chemie International Edition*, 41(12):2034-2057, 2002.

[22] Ur Rehman, H., Chen, Y., Hedenqvist, M. S., Li, H., Xue, W., Guo, Y., Guo, Y., Duan, H. and Liu, H. Self-healing shape memory PUPCL copolymer with high cycle life. *Advanced Functional Materials*, 28(7):1704109, 2018.

[23] Penfold, N. J., Yeow, J., Boyer, C. and Armes, S. P. Emerging trends in polymerization-induced self-assembly. *ACS Macro Letters*, 8(8):1029-1054, 2019.

[24] Lendlein, A. and Langer, R. Biodegradable, elastic shape-memory polymers for potential biomedical applications. *Science*, 296(5573):1673-1676, 2002.

[25] Ji, F. L., Hu, J. L., Li, T. C. and Wong, Y. W. Morphology and shape memory effect of segmented polyurethanes. Part I: With crystalline reversible phase. *Polymer*, 48(17):5133-5145, 2007.

[26] Duarah, R., Singh, Y. P., Gupta, P., Mandal, B. B. and Karak, N. High performance bio-based hyperbranched polyurethane/carbon dot-silver nanocomposite: a rapid self-expandable stent. *Biofabrication*, 8(4):045013, 2016.

[27] Duarah, R., Singh, Y. P., Gupta, P., Mandal, B. B. and Karak, N. Smart self-tightening surgical suture from a tough bio-based hyperbranched polyurethane/reduced carbon dot nanocomposite. *Biomedical Materials*, 13(4):045004, 2018.

[28] Qu, Q., He, J., Da, Y., Zhu, M., Liu, Y., Li, X., Tian, X. and Wang, H. High toughness polyurethane toward artificial muscles, tuned by mixing dynamic hard domains. *Macromolecules*, 54(17):8243-8254, 2021.

[29] Wang, X., Ao, Q., Tian, X., Fan, J., Tong, H., Hou, W. and Bai, S. Gelatin-based hydrogels for organ 3D bioprinting. *Polymers*, 9(9):401, 2017.

[30] Xiang, L. and Cui, W. Biomedical application of photo-crosslinked gelatin hydrogels. *Journal of Leather Science and Engineering*, 3:1-24, 2021.

[31] Sapuan, S. M., Pua, F. L., El-Shekeil, Y. A. and AL-Oqla, F. M. Mechanical properties of soil buried kenaf fibre reinforced thermoplastic polyurethane composites. *Materials & Design*, 50:467-470, 2013.

[32] Kay, M. J., Morton, L. H. G. and Prince, E. L. Bacterial degradation of polyester polyurethane. *International Biodeterioration*, 27(2):205-222, 1991.